

# Journal of Materials Chemistry C

Materials for optical, magnetic and electronic devices

Accepted Manuscript

This article can be cited before page numbers have been issued, to do this please use: R. Kawamura, W. He, A. Isobe, H. Zhang, N. Ikeda, Y. Hayamizu and T. Michinobu, *J. Mater. Chem. C*, 2026, DOI: 10.1039/D5TC03831F.



This is an Accepted Manuscript, which has been through the Royal Society of Chemistry peer review process and has been accepted for publication.

Accepted Manuscripts are published online shortly after acceptance, before technical editing, formatting and proof reading. Using this free service, authors can make their results available to the community, in citable form, before we publish the edited article. We will replace this Accepted Manuscript with the edited and formatted Advance Article as soon as it is available.

You can find more information about Accepted Manuscripts in the [Information for Authors](#).

Please note that technical editing may introduce minor changes to the text and/or graphics, which may alter content. The journal's standard [Terms & Conditions](#) and the [Ethical guidelines](#) still apply. In no event shall the Royal Society of Chemistry be held responsible for any errors or omissions in this Accepted Manuscript or any consequences arising from the use of any information it contains.

## Organic electrochemical transistor-based biosensors using doped polyaniline

Ryotaro Kawamura, Waner He\*, Atsushi Isobe, Haoqin Zhang, Nanase Ikeda, Yuhei Hayamizu, and Tsuyoshi Michinobu\*

Department of Materials Science and Engineering, Institute of Science Tokyo, 2-12-1  
Ookayama, Meguro-ku, Tokyo 152-8552, Japan

E-mail: he.w.ac@m.titech.ac.jp (W.H.); michinobu@mct.isct.ac.jp (T.M.)

Electronic Supplementary Information (ESI) available. See DOI: 10.1039/x0xx00000x

### Abstract

The development of high-performance biosensors is essential for advancing health monitoring in aging societies and for ensuring safety in food and environmental systems. Among various sensing platforms, organic electrochemical transistors (OECTs) stand out as especially promising because of their intrinsic signal amplification, high sensitivity, biocompatibility, and low-voltage operation. Here, we report a class of OECT-based biosensors that utilize polyaniline (PANI) films doped with 4-sulfophthalic acid (SPA) and phenol 4-sulfonic acid (PSA), achieving improved electrical conductivity from 0.2 S cm<sup>-1</sup> (pristine PANI) to 36 S cm<sup>-1</sup> (PANI-SPA) and 56 S cm<sup>-1</sup> (PANI-PSA), enhanced redox activity, and superior morphological robustness. Comprehensive characterization using transfer characteristics, cyclic voltammetry, and atomic force microscopy confirmed that the doped PANI films exhibited enhanced conductivity, surface homogeneity, and electrochemical stability. More importantly, the doped OECTs demonstrated sensitive detection of biologically relevant analytes, such as ascorbic acid (AA), uric acid (UA), and dopamine (DA). Shifts in transfer curves and changes in transconductance ( $g_{m,max}$  up to 0.19 mS for PANI-SPA with AA and 0.24 mS for PANI-PSA with DA) revealed distinct interaction profiles for each doped film-analyte pair, corresponding to strong molecular interactions and oxidation potential shifts. In summary, these findings highlight a feasible strategy for designing OECT biosensors with tunable selectivity and robust performance.



## 1. Introduction

The sensitive detection of biomolecules is critical for applications in healthcare monitoring, food safety, and environmental analysis.<sup>1,2</sup> In recent years, increasing attention has been directed toward the development of biosensing devices that are compact, flexible, and capable of operating directly on biological tissues or surfaces.<sup>3-6</sup> Among the various sensing platforms, organic electrochemical transistors (OECTs) have emerged as particularly promising owing to their intrinsic signal amplification, high sensitivity, low-voltage operation, and excellent biocompatibility.<sup>7-12</sup> In contrast to conventional organic field-effect transistors (OFETs), where charge modulation is largely confined to the interfacial region, OECTs facilitate volumetric doping throughout the entire channel.<sup>13</sup> This feature enables small gate-voltage changes to produce large variations in drain current, resulting in enhanced transconductance and signal amplification, a key advantage for biomolecule detection. In recent years, OECTs have been applied to pH sensing<sup>14</sup>, glucose detection<sup>15</sup>, and enzyme sensing<sup>16</sup>, leveraging these properties. In addition, the inherent flexibility and transparency of polymers make them highly attractive for integration into wearable sensor technologies.<sup>17</sup>

Conducting polymers serve as the essential channel materials for OECTs. Their electrical and electrochemical properties can be readily tailored through chemical functionalization or doping, providing lightweight, flexible, and cost-effective platforms for bioelectronics. Among them, poly(3,4-ethylenedioxythiophene):poly(styrene sulfonate) (PEDOT:PSS) has been widely adopted owing to its high conductivity and stability.<sup>7,18</sup> However, commercial PEDOT:PSS is typically supplied as an aqueous dispersion, which complicates device fabrication and often requires additional treatments to achieve water-insoluble films while maintaining conductivity.<sup>19</sup> Moreover, its relatively high-cost poses challenges for large-scale or disposable applications.

Polyaniline (**PANI**) presents an attractive alternative, offering low-cost precursors, straightforward polymerization, and excellent redox activity.<sup>20-22</sup> **PANI**-based OECTs have been explored for applications, such as pH sensing, ion detection, and complementary circuits.<sup>23,24</sup> However, pristine **PANI** exhibits relatively low conductivity and only moderate stability in air or aqueous environments, which limits its broader applicability.<sup>25</sup> To address these limitations, a variety of strategies have been investigated, including the incorporation of nanomaterials (e.g., graphene<sup>26</sup> and gold<sup>27</sup>) and chemical dopants.<sup>28-30</sup> Among the latter, sulfonic acids such as camphor sulfonic acid<sup>31,32</sup>, benzenesulfonic acid<sup>33</sup>, ferrocene sulfonic acid<sup>34</sup>, and polystyrene sulfonic



acid<sup>35,36</sup> have been shown to improve conductivity, stability, and mechanical robustness. Importantly, these dopants avoid the use of potentially hazardous metals, a critical consideration for biosensing applications.

In particular, 4-sulfophthalic acid (**SPA**) and phenol-4-sulfonic acid (**PSA**) have emerged as effective dopants for **PANI**.<sup>37,38</sup> Their aromatic structures and functional groups enhance film conductivity, redox activity, and thermal as well as mechanical stability. The dopant choice also influences molecular packing and hydrogen-bonding interactions, which directly impact device performance. Notably, the use of **SPA** and **PSA** enables a simplified fabrication process for high-performance OECTs, reducing reliance on complex post-treatments or hazardous substances.

Here, we report the development of **PANI**-based OECT biosensors doped with **SPA** and **PSA** for the detection of biologically relevant molecules, including ascorbic acid (**AA**), uric acid (**UA**), and dopamine (**DA**). We systematically examine how dopant type influences film morphology, electrochemical behavior, and OECT performances. Our findings demonstrate that sulfonic acid doping not only improves conductivity and stability but also enables tunable molecular interactions, offering a practical and scalable approach to high-performance and durable OECT biosensors.

## 2. Results and discussion

### 2.1. OECT performance using doped PANI

#### 2.1.1. Transfer characteristics and film morphology

The chemical structures of the materials and the OECT devices used in this study are shown in **Fig. 1**. To compare the basic electrical performance of pristine **PANI** with **SPA**- or **PSA**-doped **PANI** in OECTs, the transfer and output characteristics were first measured (**Fig. 2a-b** and **Fig. S1**). A phosphate buffer (0.1 M) was used as the electrolyte, and a fixed drain voltage ( $V_D = -0.6$  V) was applied while the gate voltage was swept from 1.0 V to  $-1.0$  V. When the applied gate voltage exceeds the threshold voltage, a conductive channel forms within the film, allowing a drain current to flow. The resulting current change is referred to as the transconductance ( $g_m$ ), one of the key parameters of an OECT. It represents the change in drain current with respect to the change in gate voltage and can be expressed as  $g_m = \Delta I_D / \Delta V_G$ . The transconductance was calculated using this relationship and plotted in the same manner (**Fig. 2b**). As shown in **Fig. 2a**, the pristine **PANI** showed the lowest drain current, reflecting its lower redox efficiency and reduced ionic transport



compared to the doped **PANI**. By introducing sulfonic acid groups, which act as more effective proton donors and enable stronger ion- $\pi$  interaction, OECTs based on **PANI-SPA** and **PANI-PSA** exhibited lower threshold voltages ( $V_{th}$ ) and higher drain currents, accompanied by increased transconductance. The conductivities of the different materials were also measured. The pristine **PANI** exhibited the lowest conductivity of  $0.2 \text{ S cm}^{-1}$ , while **PANI-PSA** showed the highest conductivity of  $56 \text{ S cm}^{-1}$ , followed by **PANI-SPA** at  $36 \text{ S cm}^{-1}$ . These results indicate that doping **PANI** with **SPA** and **PSA** effectively enhances its conductivity, which contributes to the higher transconductance observed in the corresponding OECTs compared to pristine **PANI**. The multi-peak behavior observed in the transfer characteristics (**Fig. 2b**) is most likely attributed to the intrinsic multi-step redox transitions of **PANI**, which undergoes sequential oxidation from the leucoemeraldine to the emeraldine state and further to the pernigraniline state, accompanied by proton-coupled electron transfer processes. Although heterogeneous ion penetration within the film may also contribute to peak splitting, this effect is likely minor, as suggested by the homogeneous morphology observed in the SEM images (*vide infra*).

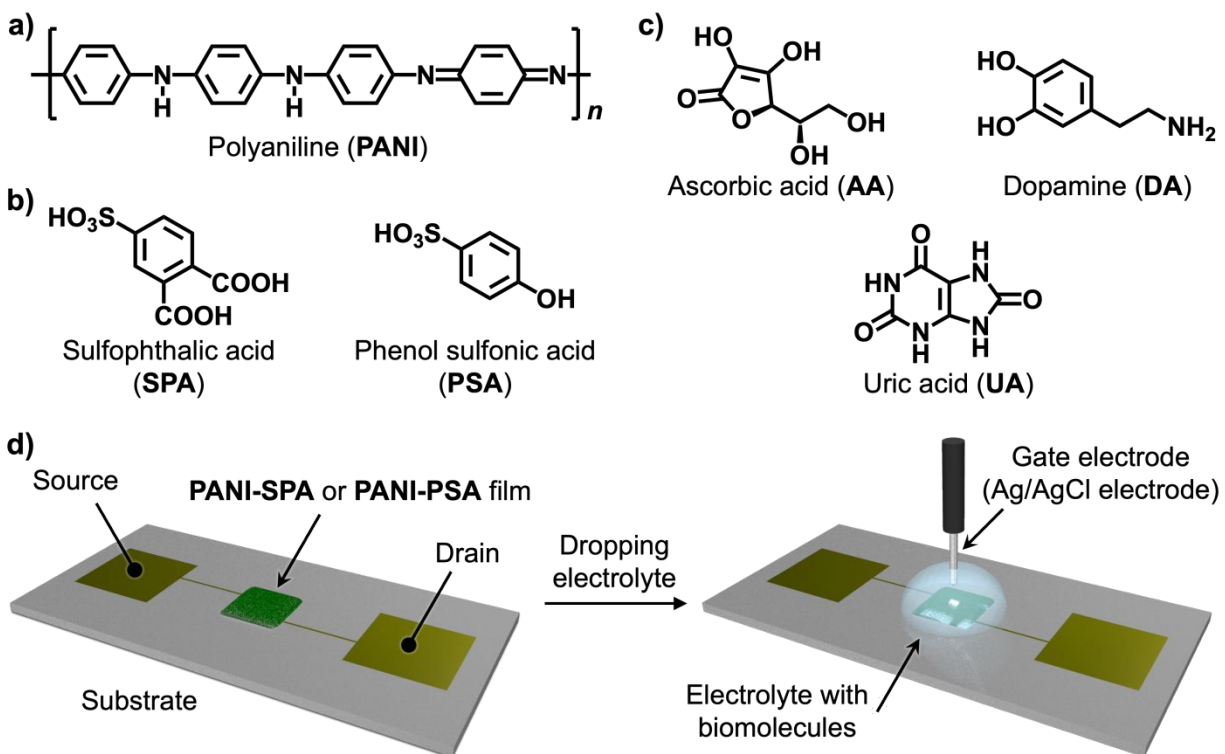


**Fig. 1** The chemical structures of a) polyaniline (PANI); b) 4-sulfophthalic acid (SPA) and phenol-4-sulfonic acid (PSA); c) ascorbic acid (AA), uric acid (UA), and dopamine (DA). d) The schematics depicting the structure of the OECT devices.

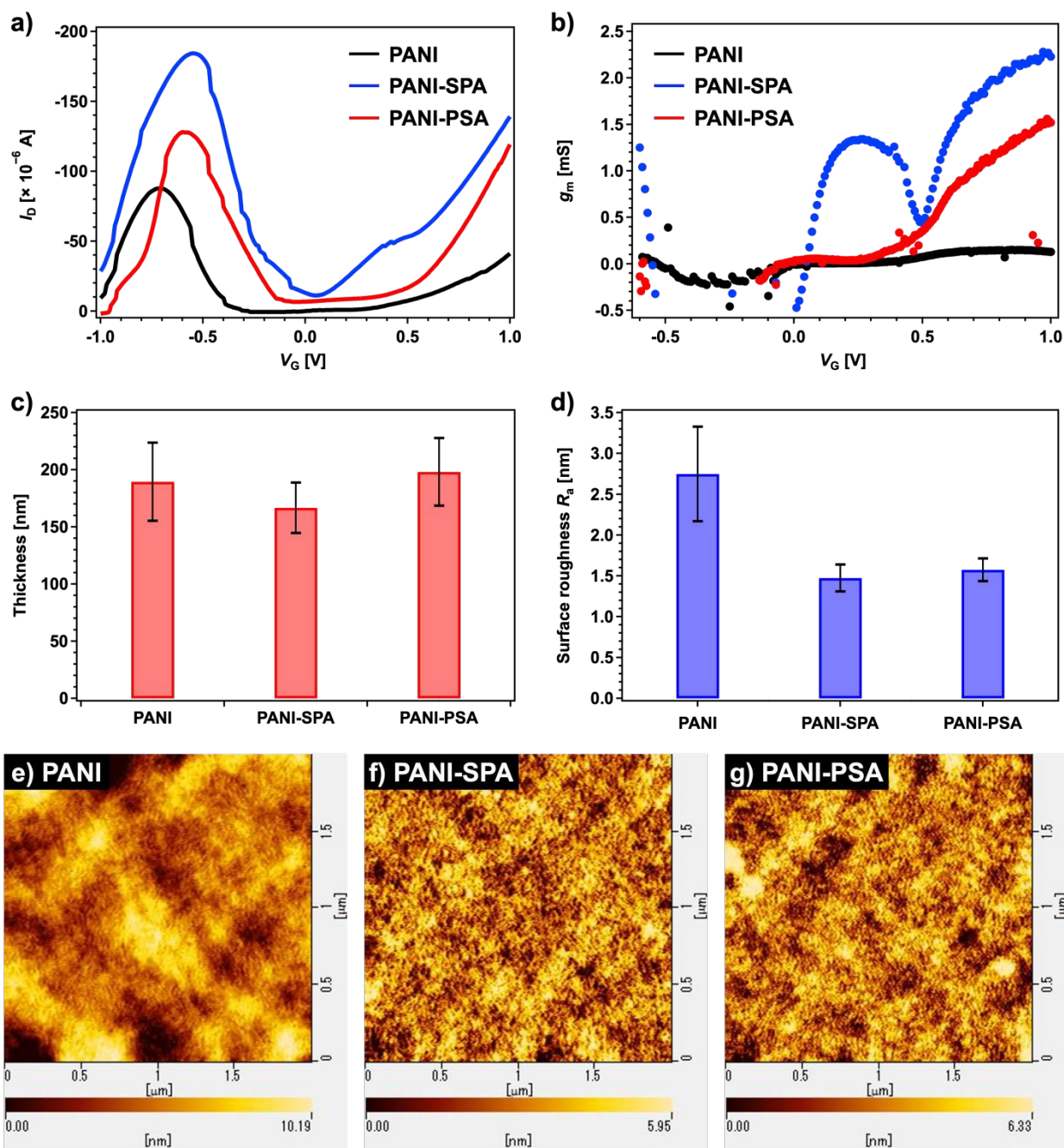


**Fig. 2** a) Transfer characteristics and b) the corresponding transconductance ( $g_m$ ) of OECTs based on PANI, PANI-SPA, and PANI-PSA at  $V_D = -0.6$  V. c) Average film thicknesses and d) average surface roughness values (RMS or  $R_a$ ), calculated from nine independent measurements across



three samples (with at least 15 data points per film). AFM height images ( $2\ \mu\text{m} \times 2\ \mu\text{m}$ ) of polymer films: e) **PANI**, f) **PANI-SPA**, and g) **PANI-PSA**.

For the OECTs, the detailed fabrication process of pristine **PANI** and doped **PANI** thin films is shown in **Fig. S2**. For the doped films, the as-prepared **PANI** layers were immersed in isopropanol containing **SPA** or **PSA** for 40 minutes in a closed container. Analysis of the film morphology provides insight into the structural changes induced by doping and helps clarify the performance differences observed in the OECTs. The surface morphology and thickness of the **PANI** films were examined by AFM to evaluate the structural effects of sulfonic acid doping (**Fig. 2c-g**). Pristine **PANI** exhibited the highest RMS roughness ( $\sim 2.6\ \text{nm}$ ), whereas the **PANI-SPA** and **PANI-PSA** films were markedly smoother, with roughness values reduced by approximately 40%. The AFM height images reveal that the pristine **PANI** surface contains larger voids and less uniform aggregation, while the doped films display denser and more homogeneous packing. This morphological densification is likely attributed to the incorporation of sulfonic acid dopants into inter-chain voids, where the  $-\text{OH}$  or  $-\text{COOH}$  groups in **SPA** and **PSA** can promote hydrogen bonding and electrostatic interactions between polyaniline chains. Such structural bridging is expected to facilitate charge transport, consistent with the higher electrical conductivity measured for the doped films. SEM images of the polymer films were consistent with the AFM images (**Fig. S3**). Cross-sectional SEM images revealed non-uniform film thicknesses of approximately  $0.6\text{--}1.1\ \mu\text{m}$ , indicating that the sulfonic acid immersion process did not significantly erode or swell the polymer films. The smoother surfaces of **PANI-SPA** and **PANI-PSA** are advantageous for OECT operation, as they enhance the uniformity of electrolyte–channel interactions and improve device stability during repeated cycling tests, which will be further discussed in a later section.

### 2.1.2. Electrochemical properties

The electrochemical properties of the **PANI**, **PANI-SPA**, and **PANI-PSA** films were evaluated by cyclic voltammetry (CV). The electrochemical cell consisted of a glassy carbon working electrode, an Ag/AgCl reference electrode, and a platinum wire counter electrode, with a phosphate buffer solution as the supporting electrolyte. CV measurements were performed over a potential window of  $1\ \text{V}$  to  $-1\ \text{V}$  at a scan rate of  $50\ \text{mV s}^{-1}$  at room temperature. Each film was tested over five consecutive cycles under these conditions.



As shown in **Fig. 3a**, the CV response of the pristine **PANI** film displays a low current density and a poorly defined redox couple, indicating limited redox reversibility and low charge carrier mobility. The unstable redox behavior observed in the CV curves of pristine **PANI** may partly result from weak adhesion between the film and the electrode surface. During cycling, particularly upon deprotonation to the emeraldine base form, partial delamination or loss of electrochemical contact likely contributes to the irregular and diminishing redox peaks. The current gradually increases across cycles, which can be attributed to incomplete film activation and slow ion diffusion within the undoped film matrix. In contrast, the **PANI-SPA** (**Fig. 3b**) and **PANI-PSA** (**Fig. 3c**) films show significantly higher redox currents and more pronounced, symmetric redox peaks, indicative of enhanced redox reversibility and improved ionic-electronic coupling. In these doped films, the first cycle shows a steep increase in current response, which then stabilizes in subsequent cycles, reflecting the rapid establishment of electrochemical equilibrium within the doped matrices. Both **SPA** and **PSA** act not only as proton donors that maintain the conductive emeraldine salt form of polyaniline, but also as sources of sulfonate anions that strongly interact with the **PANI** backbone through electrostatic interactions and  $\pi$ - $\pi$  stacking.<sup>39,40</sup> These interactions stabilize the redox-active form of **PANI**, prevent physical delamination, and enhance ion mobility and charge transfer. These results confirm that sulfonic acid doping improves the redox kinetics and ion transport properties of **PANI**, which are essential for reliable OECT performance in the previous section.

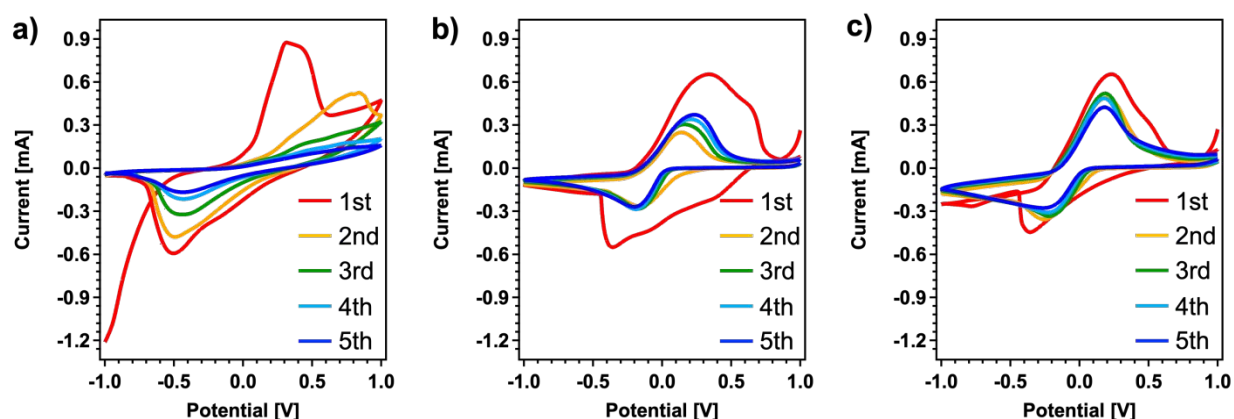


**Fig. 3** CV measurements at  $50 \text{ mV s}^{-1}$  for a) **PANI**, b) **PANI-SPA**, and c) **PANI-PSA** films fully coated on the surface of a 3 mm-diameter glassy carbon electrode over five consecutive scanning cycles. The potential was swept between  $-1 \text{ V}$  to  $+1 \text{ V}$ .



### 2.1.3. Switching stability of OECT devices

Stability performance is one of the key metrics for biosensing applications. To evaluate the dynamic switching stability of our devices as biosensors, the OECTs were subjected to repeated gate voltage pulsing (**Fig. S4** and **Fig. 4**). Based on the threshold voltage, all devices underwent alternating 20-second on/off cycles of gate voltage (0.5 V / 0 V) over a total duration of 10,000 seconds. The drain current was continuously recorded, and the steady-state current at each "on" state was extracted 20 seconds after the gate pulse to assess long-term performance. As shown in **Fig. 4a**, the pristine **PANI** device exhibited an initial drain current of approximately 0.004 mA, which gradually decreased to a value of around 0.001 mA. The corresponding current loss over time indicates cumulative degradation or partial de-doping of the channel under repeated redox cycling. This instability likely arises from insufficient ionic buffering, poor structural integrity, and weak adhesion between the film and the substrate. In contrast, **PANI-SPA** (**Fig. 4b**) and **PANI-PSA** (**Fig. 4c**) devices showed robust switching stability throughout the test, with the constant values of approximately 0.36 mA. These results suggest that doping increased the initial drain current and resulted in improved relative current retention. Therefore, incorporating the sulfonic acid is highly beneficial for enhancing the response intensity and switching stability of **PANI**-based OECTs.



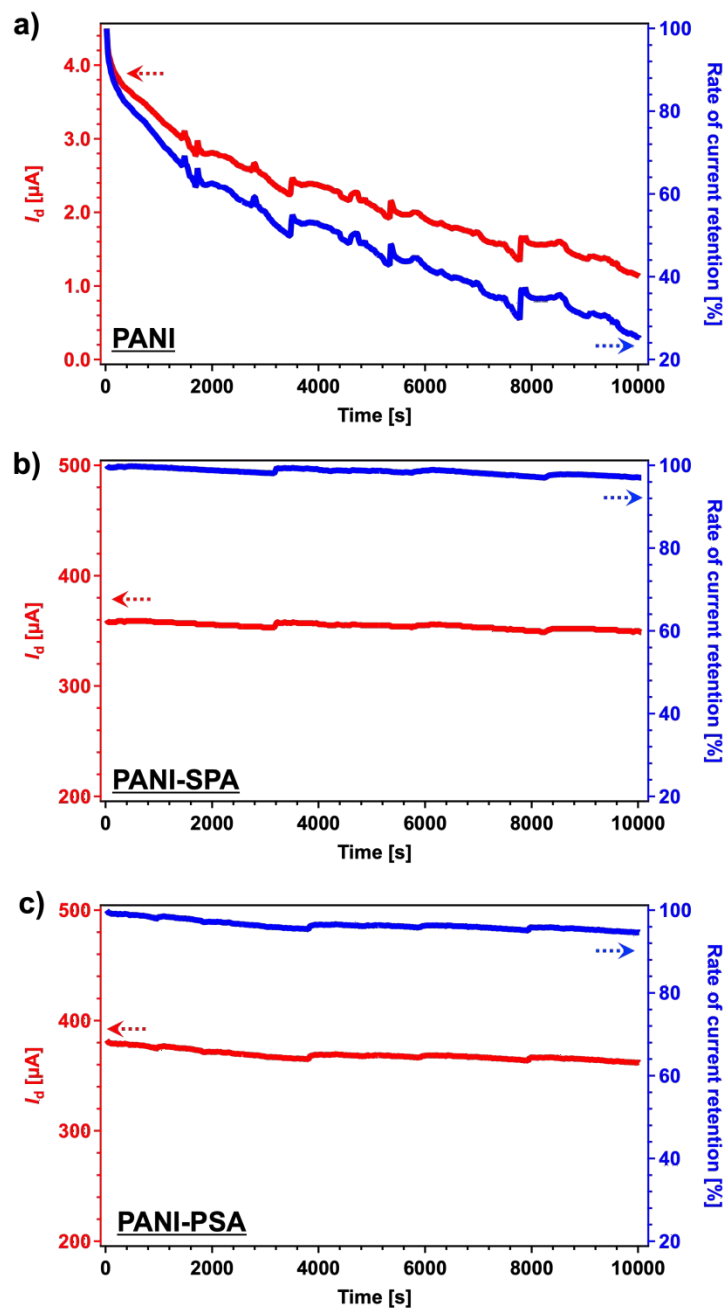


**Fig. 4** Current evolution (red) and corresponding rate of current loss (blue) of OECTs based on a) **PANI**, b) **PANI-SPA**, and c) **PANI-PSA** under repeated switching at 20 s intervals. The drain voltage was fixed at  $-0.6$  V, and a gate voltage of  $0.5$  V was applied for 20 s, followed by  $0$  V for 20 s, repeated over a total duration of 10,000 s. The current value during each "on" period was recorded 20 seconds after gate bias application to ensure a steady-state response. The current loss rate was calculated relative to the preceding cycle.



## 2.2. Detection of biomolecules using polyaniline-based OECTs

### 2.2.1. Responses toward AA, UA, and DA

To evaluate the sensing capability of polyaniline-based OECTs, we investigated their responses to three representative redox-active biomolecules, namely, ascorbic acid (AA), uric acid (UA), and dopamine (DA), each at 1 mM in phosphate buffer (PBS, 0.1 M, pH 7). Transfer curves were recorded at a fixed drain voltage of  $-0.6$  V (Fig. S5), and the corresponding transconductance was extracted over the voltage range of  $-0.3$  V to  $0.7$  V (Fig. 5). Comparisons were made among the PANI, PANI-SPA, and PANI-PSA films used in this study. All measurements were conducted at least four times under identical operating conditions using a minimum of two OECT devices fabricated via the same process. For the transfer characteristics, the average of at least five transfer curves from reliable measurements was used. Table S1 summarizes the maximum transconductance values ( $g_{m,max}$ ), the gate voltage at  $g_{m,max}$ , and the corresponding threshold voltages.

For pristine PANI (Fig. 5a), all three biomolecules increased  $g_m$  relative to PBS, with UA producing the largest enhancement along with a lower threshold voltage. This likely reflects the relatively hydrophobic nature of UA, which promotes stronger interaction with the less compact, hydrophobic PANI surface. However, the relatively high  $g_m$  observed even in PBS, combined with the small  $\Delta g_m$  upon analyte addition, suggests poor signal specificity and thus limits sensing resolution. In contrast, for PANI-SPA (Fig. 5b), AA induced a pronounced  $g_m$  increase ( $g_{m,max} = 0.19$  mS) accompanied by a large negative shift in threshold voltage ( $-0.12$  V), indicating facilitated channel doping at lower potentials. This behavior can be attributed to strong hydrogen-bonding and  $\pi$ - $\pi$  interactions between AA and the carboxyl-bearing sulfonic acid dopant, which also lowers AA's oxidation potential. In contrast, UA and DA produced smaller  $g_m$  changes and threshold shifts comparable to that observed with PBS alone. For PANI-PSA (Fig. 5c), all three biomolecules lowered the threshold voltages. Moreover, both AA and DA induced substantial  $g_m$  enhancements, with DA exhibiting the highest  $g_m$  ( $0.24$  mS) and a slightly lower threshold voltage than AA. This suggests that the phenolic groups of the dopant provide additional  $\pi$ - $\pi$  and electrostatic interactions that favor catecholamine binding, while AA benefits from similar hydrogen-bonding effects as observed in PANI-SPA. In contrast, UA again showed only a minimal response and a higher threshold voltage compared to AA and DA, likely due to reduced interfacial compatibility.



Therefore, sulfonic acid doping enhances sensing selectivity by introducing functional groups capable of specific hydrogen-bonding or  $\pi$ - $\pi$  interactions with target biomolecules. **PANI-SPA** displays pronounced specificity toward **AA**, whereas **PANI-PSA** strongly responds to both **AA** and **DA**. These differentiated response patterns highlight their potential for selective biosensing applications, where redox potential shifts and  $g_m$  enhancement can be leveraged for molecular discrimination.

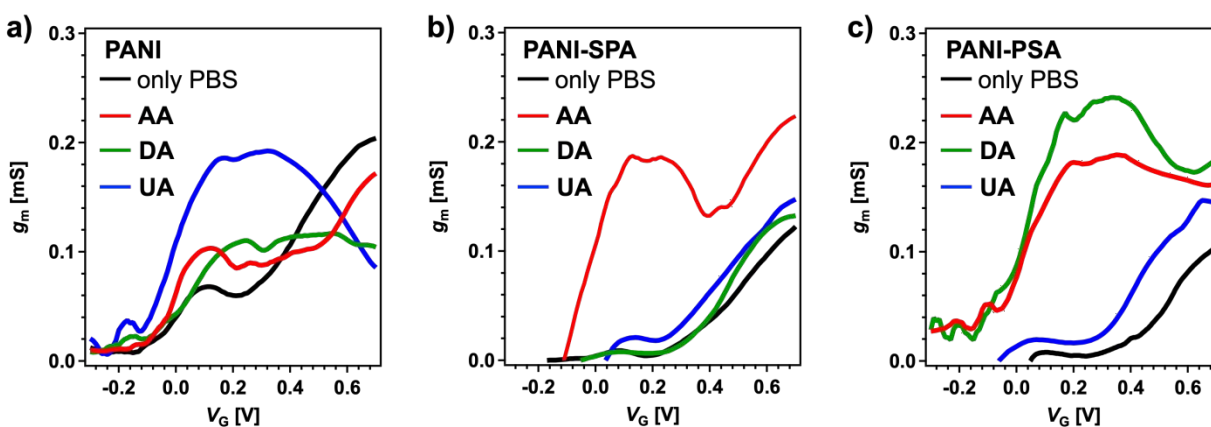


**Fig. 5** Transconductance responses of a) **PANI**, b) **PANI-SPA**, and c) **PANI-PSA** OECTs in the presence of ascorbic acid (**AA**, red), dopamine (**DA**, green), and uric acid (**UA**, blue) at 1 mM in phosphate buffer solution (PBS, 0.1 M, pH 7), compared to PBS alone (black). Measurements were performed at  $V_D = -0.6$  V with  $V_G$  swept from  $-0.3$  to  $0.7$  V.

### 2.2.2. Concentration dependence

Based on the biomolecule response analysis, **PANI-SPA** OECTs exhibited strong selectivity toward **AA**, while **PANI-PSA** devices showed high sensitivity to both **AA** and **DA**. For practical biosensing applications, however, quantitative detection across varying analyte concentrations is essential. To this end, we systematically investigated the influence of biomolecule concentration on the electrical characteristics of these OECTs. **Fig. S6** and **Fig. 6** present the evolution of transfer curves and transconductance profiles across concentrations ranging from 1  $\mu$ M to 10 mM. The results of transfer and  $g_m$  characteristics are summarized using the average plots of at least five reliable original transfer curves, as described in section 2.2.1. **Table S2** provides a comparison of  $g_{m,max}$ , the corresponding gate voltage at  $g_{m,max}$ , and the associated threshold voltage for the OECT sensors.



As shown in **Fig. 6a, 6d** and **Table S2**, **PANI-SPA** OECTs exhibited a clear concentration-dependent response to **AA** over the tested range (1  $\mu\text{M}$ –10 mM). Even at 1  $\mu\text{M}$ , a pronounced increase in drain current and transconductance was observed, with  $g_{m,max}$  rising steadily as the **AA** concentration increased. The corresponding gate voltage at  $g_{m,max}$  remained confined within a narrow low-potential window ( $\sim 0.08$ – $0.15$  V), enabling selective **AA** detection at voltages substantially lower than those typically reported for PEDOT:PSS-based sensors.<sup>41,42</sup> The progressive negative shift in threshold voltage with higher **AA** concentrations further supports enhanced carrier injection efficiency at low potentials, which can be leveraged for high-sensitivity **AA** quantification within physiological ranges. Mechanistically, sulfonic acid doping in **PANI-SPA** likely facilitates more efficient **AA** oxidation by lowering its redox potential, thereby promoting earlier channel dedoping and amplifying transconductance at low gate bias.

For **PANI-PSA**, the response to **AA** was also strong, with  $g_{m,max}$  values already high (0.16 mS) at 1  $\mu\text{M}$ , indicating a high intrinsic affinity between the phenol sulfonic acid-doped polymer and **AA** (**Fig. 6b** and **6e**). However, the increase in  $g_{m,max}$  with concentration was modest ( $\Delta g_{m,max} \approx 0.01$  mS from 1  $\mu\text{M}$  to 1 mM), and the gate voltage at  $g_{m,max}$  shifted to higher values as the concentration increased. These trends suggest that while **PANI-PSA** enables rapid responses at low concentrations, the limited number of available reaction sites on its relatively compact surface may lead to early saturation, reducing the impact of further concentration increases. The broader  $g_{m,max}$  voltage range (0.17–0.36 V) further suggests slower kinetics or delayed peak channel modulation at higher **AA** loadings. For **DA** sensing with **PANI-PSA**, concentration-dependent responses were also evident down to 1  $\mu\text{M}$ , with  $g_{m,max}$  reaching a maximum of  $\sim 0.25$  mS at 100  $\mu\text{M}$  (**Fig. 6c** and **6f**). The lack of further enhancement at 1 mM and the subsequent decline at 10 mM likely arise from redox byproduct accumulation or electrode fouling, which introduce parasitic resistances and hinder ionic transport. Unlike **AA**, **DA** maintained relatively stable gate voltage positions for  $g_{m,max}$  (0.26–0.37 V) across the tested range, indicating that **DA** oxidation kinetics and charge transfer processes at the polymer interface are less sensitive to gate potentials.

These results indicate that the **PANI-SPA** architecture is optimal for quantitative **AA** sensing at low gate voltages, offering high selectivity, while **PANI-PSA** enables dual-analyte detection (**AA** and **DA**) with high sensitivity in the sub-100  $\mu\text{M}$  range but exhibits signal saturation and redox interference at higher concentrations. Collectively, these findings highlight the inherent trade-off between sensitivity and dynamic range in doped-**PANI** OECTs and underscore the



importance of surface and interface engineering to extend the linear sensing range without compromising low-voltage operation.

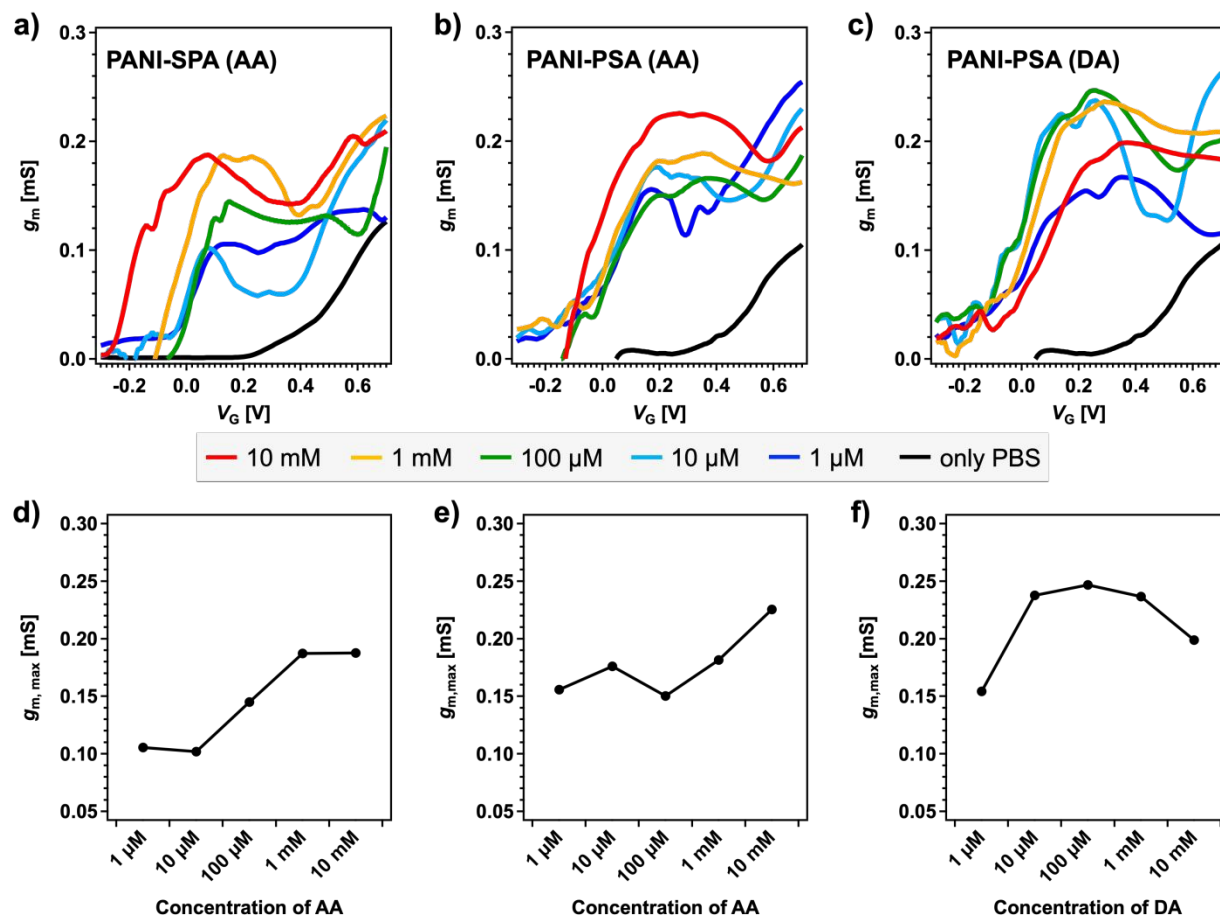


**Fig. 6** Transconductance responses in OECTs of a) PANI-SPA to varying AA concentrations and b,c) PANI-PA to b) AA and c) DA. Maximum transconductance values in the range of 0–0.4 V under different analyte concentrations: d) PANI-SPA for AA; e) PANI-PSA for AA, and f) PANI-PSA for DA. Analyte concentrations were 0, 1  $\mu$ M, 10  $\mu$ M, 0.1 mM, 1 mM, and 10 mM in 0.1 M PBS.

## 2.3. Effects of sulfonic acid

### 2.3.1. Electrochemical measurements

To evaluate the origin of the sensing differences observed in OECTs, electrochemical measurements were performed to investigate the direct interactions between sulfonic acids (SPA and PSA) and the biomolecules. CV and differential pulse voltammetry (DPV) measurements were



performed in PBS electrolytes (0.1 M, 15 mL) containing 1 mM biomolecule, with or without the addition of 1 mL **SPA** or **PSA** solution. The electrode setup consisted of a GCE working electrode, an Ag/AgCl reference electrode, and a Pt counter electrode. CV scans were recorded over a potential range of  $-1.0$  V and  $1.0$  V at a scan rate of  $0.05$  V/s for five consecutive cycles, while DPV measurements were conducted with a pulse amplitude of  $0.025$  V, a pulse width of  $0.06$  ms, and an interval of  $0.5$  s. Representative stabilized scans are shown in **Fig. 7** and **S7-S8**.

As shown in **Fig. 7a**, the baseline CVs recorded without biomolecules showed small but consistent shifts in current response across the potential window upon addition of sulfonic acids. The background PBS-derived reduction peak shifted toward more negative potentials ( $\text{PBS} < \text{SPA} < \text{PSA}$ ), indicating a direct perturbation of the electrolyte environment. However, the current magnitude remained less than 10% of that observed for polyaniline-coated films, suggesting that **SPA** and **PSA** themselves do not substantially contribute to redox activity.

When biomolecules were introduced, distinct shifts in the anodic peak positions were observed, consistent with their intrinsic oxidation potentials (**Fig. 7b** and **S7**). For **AA** (**Fig. 7b**), the anodic peak shifted to more negative

potentials in the presence of **SPA**, while **PSA** produced only a minimal effect, causing a slight positive shift. This indicates a specific interaction between **SPA** and **AA** that lowers the oxidation potential, consistent with the enhanced **AA** selectivity of **PANI-SPA** OECTs. To further confirm the effect, **UA** and **DA** were also measured in the same conditions. Both **DA** and **UA** produced characteristic peaks compared with the PBS-only controls. These CV results suggest that sulfonic acids modulate the electron transfer energetics in a biomolecule-dependent manner, but the magnitude of these effects remains modest at the CV scale.

DPV measurements (**Fig. S8**) further clarified these differences with higher resolution. In PBS alone, the oxidation peaks for **AA**, **UA**, and **DA** were well separated. Compared with the baseline oxidation peaks observed without biomolecules ( $\approx -0.2$  to  $0.2$  V, **Fig. S8a**), **AA** exhibited oxidation peaks at more positive potentials ( $\approx 0.05$  to  $0.35$  V, **Fig. S8b**), followed by **DA** ( $\approx 0.05$  to  $0.25$  V), while **UA** required even higher potentials ( $\approx 0.25$  to  $0.4$  V). Notably, for **UA**, an additional oxidation peak at the same position as in **Fig. S8a** was still observed. These findings indicate that **AA** and **DA** are more readily oxidized and suppress the oxidation of **PSA** and **SPA** (relative to **UA**), consistent with their lower redox potentials and their easily detectable responses in OECTs.



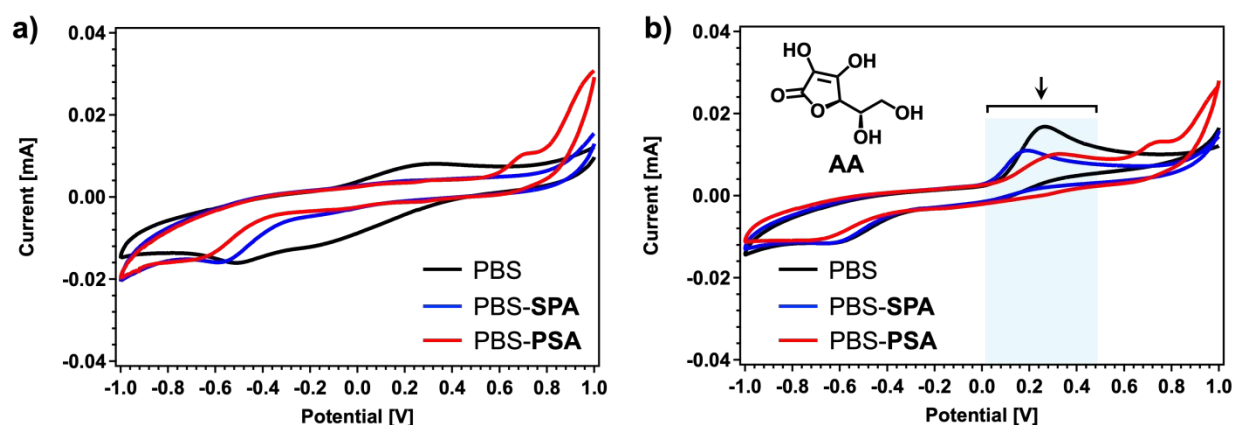


**Fig. 7** Cyclic voltammograms of electrolytes containing a) only PBS and b) 1 mM AA, measured in PBS (black), PBS + SPA (blue), and PBS + PSA (red). Measurements were performed using a GCE working electrode, an Ag/AgCl reference, and a Pt counter electrode. The potential was scanned from  $-1.0$  V to  $1.0$  V at  $50$   $\text{mV s}^{-1}$ . The curves shown correspond to the second cycle, after stabilization during the first scan.

### 2.3.2. FT-IR and Raman measurements

To further investigate the interactions between sulfonic acid dopants and the target biomolecules beyond their electrochemical effects, Fourier-transform infrared (FT-IR) spectroscopy was measured. Specifically, potential bonding or hydrogen-bonding interactions between functional groups were examined. For these measurements, 5 mL of deionized water containing 1 mM of AA, DA, or UA was prepared. Subsequently, 300  $\mu\text{L}$  of sulfonic acid solution (SPA or PSA) was added, and the mixture was stirred prior to analysis.

The full spectra are presented in **Fig. S9**. Owing to the aqueous solvent, a broad absorption band around  $3300$   $\text{cm}^{-1}$  and a peak at  $1640$   $\text{cm}^{-1}$  were observed, corresponding to O-H stretching and H-O-H bending of water, respectively. **Fig. 8** shows the expanded region of  $900$ – $1500$   $\text{cm}^{-1}$ , highlighting key vibrational features relevant to biomolecule-dopant interactions. For the SPA samples, the spectral features of all three biomolecules closely matched their respective references, indicating minimal interaction between SPA and the biomolecules. Similarly, the PSA-related samples showed negligible shifts for AA and UA. Interestingly, for DA in the presence of PSA, all characteristic peaks exhibited a small red shift ( $\sim 5$ – $6$   $\text{cm}^{-1}$ ), suggesting restricted vibrational freedom, likely due to hydrogen bonding between the phenolic group of PSA and the amino group



of **DA**. This subtle yet consistent shift implies enhanced local dielectric effects in the **PSA-DA** mixture, which could facilitate improved ionic-electronic coupling and partially account for the pronounced transconductance increase observed in **PANI-PSA** OECTs upon **DA** exposure. Importantly, no significant interactions were observed for the other biomolecule-dopant combinations, confirming that polyaniline itself is primarily responsible for biomolecule oxidation and the resulting modulation of device current. The FT-IR analysis supports that hydrogen bonding between **DA** and **PSA** selectively alters the dielectric environment, thereby modulating OECT transfer characteristics, while other sulfonic acid-biomolecule interactions remain negligible.

Furthermore, Raman spectra were collected to investigate the **PANI**-biomolecule interactions. Both **PANI-SPA** and **PANI-PSA** films showed sharp C=C bands at approximately  $1600\text{ cm}^{-1}$  and weak N-H/O-H bands in the higher wavenumber region (**Fig. S10**). Upon the addition of biomolecules, such as **AA**, **DA**, or **UA**, these characteristic bands became significantly broadened (**Fig. S10a** and **S10b**). A comparable spectral broadening was also observed when the doped **PANI** films were exposed to water vapor (**Fig. S10c** and **S10d**). These observations suggest the presence of hydrogen bonds between **SPA/PSA** and the biomolecules, but it remains difficult to quantify the strength of their interactions.

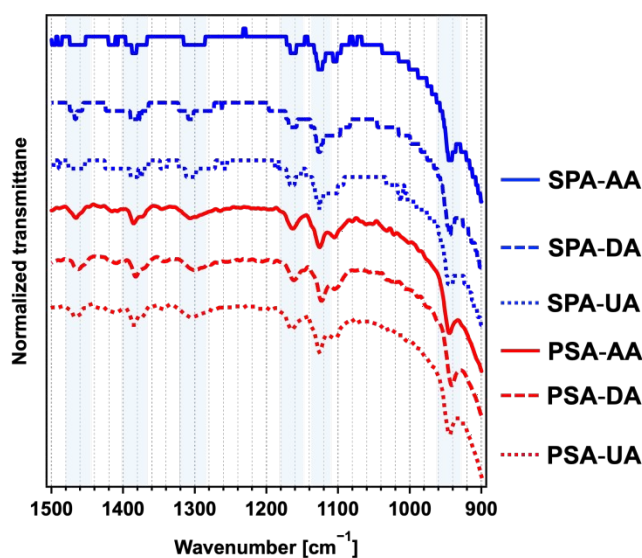


**Fig. 8** FT-IR spectra of biomolecule-sulfonic acid mixtures in deionized water. Solutions containing 1 mM biomolecules (**AA**, **DA**, **UA**) with a small amount of **SPA** or **PSA** added. Key vibrational features in the  $900\text{--}1500\text{ cm}^{-1}$  region are highlighted to reveal potential hydrogen-bonding interactions.



### 3. Experimental section

#### 3.1 Materials

The key materials used in this study are shown in **Fig. 1a-c**. The conductive polymer used in this study was polyaniline (**PANI**), kindly supplied by Idemitsu Kosan Co., Ltd., as a polyaniline mother solution (HT-3, referred to as Solution A).<sup>43</sup> This solution contained approximately 5 wt% **PANI**, with a solvent system of 95 vol% toluene and 5 vol% isopropanol. This solvent system was chosen by the supplier to provide stable **PANI** dispersion and favorable spin-coating film formation, as the low volatility of toluene and small fraction of isopropanol assist in achieving uniform films. Three sulfonic acid-based dopant solutions were prepared for chemical modification of the **PANI** matrix: (i) Solution B: Naphthalene sulfonic acid solution containing 1~15 vol% naphthalenesulfonic acid in 1-propanol (85~99 vol%); (ii) Solution C1: 4-Sulfophthalic acid (**SPA**) solution composed of 0.1~5 vol% 4-sulfophthalic acid in isopropanol (95~99.9 vol%); (iii) Solution C2: Phenol sulfonic acid solution consisting of 0.1~5 vol% phenol-4-sulfonic acid (**PSA**) in isopropanol (95~99.9 vol%). All reagents were used without further purification. The electrolyte employed for device testing was 0.1 M phosphate-buffered saline (PBS, pH 7.0), acquired from Wako Pure Chemicals (Cat. No. 168-27155). Three biologically relevant analytes were all purchased from Kanto Chemical Co., Ltd. and selected for sensor evaluation: L-ascorbic acid (**AA**), special grade (01452-30); uric acid (**UA**), special grade (43013-30); dopamine hydrochloride (**DA**), special grade (10761-60).

#### 3.2 Fabrication of PANI-based OECTs

OECTs were fabricated by depositing **PANI** films onto the pre-patterned electrode substrates (BAS Inc., Japan). The film fabrication process involved surface treatment, polymer film deposition, and acid doping, as outlined below. (i) Surface treatment: Pre-patterned electrode substrates were first treated with UV-Ozone (TECHNOVISION, INC., Model 208 UV-O<sub>3</sub> cleaning system) for 10 minutes to enhance surface energy and remove organic contaminants. This was followed by sequential ultrasonic cleaning in deionized water (DI water), electronic-grade (EL) acetone, and EL isopropanol for 10 minutes each. The cleaned substrates were then dried under air flow. (ii) Polymer film deposition: **PANI** films were deposited by spin-coating a doped solution onto the cleaned substrates. The spin-coating solution was prepared by adding 38 mg of



naphthalene sulfonic acid solution (*Solution B*) to 1 g of Idemitsu **PANI** solution (*Solution A*). The mixture was stirred in an oil bath at 30 °C for 30 minutes to ensure homogeneous doping. Subsequently, 70  $\mu\text{L}$  of the prepared solution was drop-cast onto each substrate and spin-coated at 3000 rpm for 20 s. The coated substrates were then annealed at 135 °C for 30 minutes to remove residual solvents and promote internal crystallization of the **PANI** matrix. (iii) Acid doping: To enable ion exchange of the dopant and tailor electrochemical properties, the **PANI** films were subjected to a secondary doping process using either *Solution C1* or *Solution C2*. Immediately after the initial annealing, substrates were immersed in isopropanol solutions of **SPA** (*Solution C1*) or **PSA** (*Solution C2*) for 40 mins to replace naphthalene sulfonic acid anions with stronger sulfonic acid dopants. After doping, the films were briefly rinsed in isopropanol for 10 s to remove surface-bound excess dopants, dried by air-blowing, and subjected to a secondary annealing at 135 °C for 10 mins to remove residual solvent and stabilize the film morphology. As a control, **PANI**-only devices (undoped with naphthalene sulfonic acid) were fabricated using the same procedure but omitting *Solution B*. These control devices were considered complete after the initial spin-coating and annealing steps. A detailed fabrication procedure of the **PANI** films for OECTs is provided in **Fig. S1**.

### 3.3 AFM measurements

The film morphologies and thickness in this study were examined using an AFM system (Seiko Instruments SPA-400) with a stiff cantilever (Seiko Instruments DF-20).

### 3.4 SEM measurements

The surface and cross-sections of the polymer films were observed by a field emission scanning electron microscope (FE-SEM, JSM-7500F, JEOL).

### 3.5 Electrical measurements

Commercial pre-patterned electrode substrates (without connector sheets) were used as the source-drain electrodes for the OECT, as mentioned in section 4.2. An aqueous Ag/AgCl reference electrode (BAS Inc., Japan, RE-1B) served as the gate electrode in all experiments. All electrical measurements were performed under ambient conditions at room temperature. Care was taken to minimize external disturbances such as vibration and airflow during device operation. A Keithley



4200A-SCS parameter analyzer was used for all electrical characterizations, including transfer measurements, switching stability, and real-time biosensing. To record transfer curves, the OECT was configured with a constant drain voltage ( $V_D = -0.6$  V) applied between the source and drain electrodes. A droplet of 0.1 M PBS (pH 7.0) was placed over the channel to serve as the electrolyte, into which the Ag/AgCl gate electrode was immersed.  $V_G$  was swept from 1.0 V to  $-1.0$  V, and  $I_D$  was recorded throughout the  $V_G$  sweep. For sensing performance evaluation, fixed concentrations of **AA**, **UA**, or **DA** were added to the PBS electrolyte, and the transfer characteristics were measured under the same conditions. Transfer curves were compared across three device types: pristine **PANI**, **PANI-SPA**, and **PANI-PSA**. To assess dynamic switching behavior,  $V_G$  was alternated between 0 V and 0.5 V at 20 s intervals for a total duration of 1200 s. The selected  $V_G = 0.5$  V corresponds to the voltage range where the **PANI** channel exceeds its threshold voltage and enters the conducting regime. All other conditions ( $V_D$ , electrolyte, gate contact) matched those used during the transfer curve measurements.

### 3.6 CV measurements

CV experiments were performed using a model 612C electrochemical analyzer (ALS Co., Ltd., Japan). A standard three-electrode cell configuration was employed: a glassy carbon electrode (3 mm-diameter) was used as the working electrode; an Ag/AgCl electrode (in saturated KCl) served as the reference electrode; a platinum (Pt) wire was used as the counter electrode. The electrolyte used was 0.1 M PBS (pH 7.0), identical to that used for OECT electrical characterization. The polymer films were formed by drop-casting the polymer solutions with the dopant compositions similar to the OECTs on the working electrode. All CV scans were performed over a potential range of 1.0 V to  $-1.0$  V (vs. Ag/AgCl) at a scan rate of  $50 \text{ mV s}^{-1}$ , chosen to balance signal resolution with redox stability.

### 3.7 FT-IR and Raman measurements

Attenuated total reflection (ATR) FT-IR spectroscopy was measured on a JASCO FT/IR 4200 spectrometer to investigate potential interactions between sulfonic acid dopants and target biomolecules. Analyte solutions were prepared by dissolving **AA**, **DA**, or **UA** in 5 mL of deionized water to achieve a final concentration of 1 mM. To each analyte solution, 300  $\mu\text{L}$  of sulfonic acid dopant solution (either **SPA** (*Solution C1*) or **PSA** (*Solution C2*)) was added, followed by stirring



to ensure homogeneous mixing. For FT-IR measurements, approximately two drops of the mixed solution were placed on the sample stage. Spectra were collected using an accumulation of 16 scans to improve the signal-to-noise ratio. Raman spectra were measured using a custom-built micro-Raman measurement system equipped with a high-resolution spectrometer (IsoPlane, Teledyne). **PANI-PSA** and **PANI-SPA** were prepared by the same procedures as OECT fabrication. Subsequently, the saturated aqueous solution of **AA**, **DA**, or **UA** was dropped onto the film. The films in wet state were measured after exposing them to water vapor.

#### 4. Conclusion

In this work, we demonstrated the design and characterization of OECT-based biosensors employing polyaniline (**PANI**) films doped with sulfonic acids (**SPA** and **PSA**), providing a versatile strategy to tune both the electrochemical and molecular interactions in **PANI**-based OECTs. Doping **PANI** with these functional acids significantly enhanced film conductivity, morphological uniformity, and electrochemical stability, leading to improved OECT performance, including higher transconductance, lower threshold voltage, and superior switching stability. Detailed electrochemical analyses, including CV and DPV, revealed that sulfonic acid dopants can modulate the oxidation potentials of biologically relevant analytes, enabling tunable sensing responses. FT-IR characterization further confirmed that hydrogen-bonding interactions, particularly between **PSA** and **DA**, enhance the dielectric properties, facilitating efficient charge transport and selective signal amplification. This approach enables selective, sensitive, and stable detection of biomolecules such as **AA**, **UA**, and **DA**, making it a promising strategy for next-generation bioelectronic sensors with tailored selectivity and robust operational stability.

Looking forward, our future work will focus on improving operational stability during long-term cycling, evaluating limits of detection at clinically relevant concentrations, and integrating these devices into miniaturized and flexible platforms for practical point-of-care and wearable biosensing applications. By systematically optimizing both material interfaces and device architecture, doped **PANI**-based OFETs could evolve into robust and scalable sensors for real-time health and environmental monitoring.

#### Author contributions



R. K.: Investigation and writing – original draft; W. H.: Formal analysis, funding acquisition, and writing – original draft; A. I.: Project administration and writing – review and editing; H. Z.: Investigation; N. I.: Investigation; Y. H.: Project administration; T. M.: Conceptualization, supervision, funding acquisition, and writing – review and editing.

### Conflicts of interest

The authors have no conflicts of interest.

### Acknowledgements

This study was partly supported by JSPS KAKENHI Grant Number JP24H00005 (T.M.). W.H. thanks Grant-in-Aid for JSPS Fellows (23KF0223). We thank the Core Facility Center, Institute of Science Tokyo for SEM observations.

### References

- 1 N. Wang, A. Yang, Y. Fu, Y. Li and F. Yan, *Acc. Chem. Res.*, 2019, **52**, 277-287.
- 2 F. H. Awlqadr, A. B. Altemimi, S. A. Qadir, T. A. Hama Salih, Z. T. Alkanan, Q. H. AlKaisy, O. A. Mohammed and M. A. Hesarinejad, *Heliyon*, 2025, **11**, e41181.
- 3 T. Kajisa, W. Li and T. Michinobu, *ACS Omega*, 2018, **3**, 6719-6727.
- 4 T. Kajisa, W. Li, T. Michinobu and T. Sakata, *Biosens. Bioelectron.*, 2019, **117**, 810-817.
- 5 M. Xu, D. Obodo and V. K. Yadavalli, *Biosens. Bioelectron.*, 2019, **124-125**, 96-114.
- 6 Z. Zhu, Y. Pang, Y. Li, Y. Gu, X. Wang, A. Yu, B. Liu, S. Liu, W. Huang and Q. Zhao, *ACS Nano*, 2025, **19**, 4084-4120.
- 7 I. Gualandi, D. Tonelli, F. Mariani, E. Scavetta, M. Marzocchi and B. Fraboni, *Sci. Rep.*, 2016, **6**, 35419.
- 8 X. Xi, D. Wu, W. Ji, S. Zhang, W. Tang, Y. Su, X. Guo and R. Liu, *Adv. Funct. Mater.*, 2020, **30**, 1905361.
- 9 W. He, Y. Kashino, N. Nozaki, J. Kimpel, H. Matsumoto, Y. Hayamizu and T. Michinobu, *J. Mater. Chem. C*, 2024, **12**, 18282-18290.
- 10 Z. Zhu, Y. Pang, Y. Li, Y. Gu, X. Wang, A. Yu, B. Liu, S. Liu, and W. Huang, *ACS Nano*, 2025, **19**, 4084-4120.
- 11 L. Travaglini, K. Fidanovski, and D. Mawad, *Adv. Sci.*, 2025, **12**, e14448.
- 12 J. Y. Gerasimov, M. J. Donahue, D. Gao, D. Tu, and S. Fabiano, *Chem. Rev.*, 2026, **126**, 28-79.
- 13 R. Wu, M. Matta, B. D. Paulsen and J. Rivnay, *Chem. Rev.*, 2022, **122**, 4493-4551.
- 14 G. Scheiblin, R. Coppard, R. M. Owens, P. Mailley and G. G. Malliaras, *Adv. Mater. Technol.*, 2017, **2**, 1600141.
- 15 H. Tang, F. Yan, P. Lin, J. Xu and H. L. W. Chan, *Adv. Funct. Mater.*, 2011, **21**, 2264-2272.



- 16 S. Wustoni, A. Savva, R. Sun, E. Bihar and S. Inal, *Adv. Mater. Interfaces*, 2019, **6**, 1800928.
- 17 Kenry, J. C. Yeo and C. T. Lim, *Microsyst. Nanoeng.*, 2016, **2**, 16043.
- 18 H. S. White, G. P. Kittlesen and M. S. Wrighton, *J. Am. Chem. Soc.*, 1984, **106**, 5375-5377.
- 19 S. Doshi, M. O. A. Forner, P. Wang, S. E. Hadwe, A. T. Jin, G. Dijk, K. Brinson, J. Lim, A. Dominguez-Alfaro, C. Y. J. Lim, A. Salleo, D. G. Barone, G. Hong, M. L. Brongersma, N. A. Melosh, G. G. Malliaras and S. T. Keene, *Adv. Mater.*, 2025, **37**, 2415827.
- 20 J. Ouyang, C.-W. Chu, F.-C. Chen, Q. Xu and Y. Yang, *Adv. Funct. Mater.*, 2005, **15**, 203-205.
- 21 M. ElMahmoudy, S. Inal, A. Charrier, I. Uguz, G. G. Malliaras and S. Sanaur, *Macromol. Mater. Eng.*, 2017, **302**, 1600497.
- 22 T. Amaya and Y. Otake, *Bull. Chem. Soc. Jpn.*, 2025, **98**, uoaf033.
- 23 B. Fang, J. Yan, D. Chang, J. Piao, K. M. Ma, Q. Gu, P. Gao, Y. Chai and X. Tao, *Nat. Commun.*, 2022, **13**, 2101.
- 24 R. Kawamura and T. Michinobu, *Polymers*, 2023, **15**, 4657.
- 25 Z. Lu, K. Xu, K. Xiao, Q. Xu, L. Wang, P. Li, J. Zhou, D. Zhao, L. Bai, Y. Cheng and W. Huang, *Npj Flex. Electron.*, 2025, **9**, 9.
- 26 B. Chethan, V. Prasad, S. Mathew and H. Jan, *Synth. Met.*, 2024, **307**, 117644.
- 27 N. Shoaie, M. Daneshpour, M. Azimzadeh, S. Mahshid, S. M. Khoshfetrat, F. Jahanpeyma, A. Gholaminejad, K. Omidfar and M. Foruzandeh, *Mikrochim. Acta*, 2019, **186**, 465.
- 28 Y. Wang, Y. Zhang, Y. Wang, R. Zhu, Y. Chen, X. Liu, J. Xu, M. Li and D. Wang, *Electroanalysis*, 2021, **33**, 2406-2416.
- 29 H. J. N. P. D. Mello, M. C. Faleiros and M. Mulato, *Electrochem. Sci. Adv.*, 2022, **2**, e2100176.
- 30 Z. Ma, H. Sun, K. Xiao, J. Dong, S. Wang, L. Wang, P. Li and K. Xu, *Microchim. Acta*, 2024, **191**, 391.
- 31 J. P. Pouget, C. H. Hsu, A. G. MacDiarmid and A. J. Epstein, *Synth. Met.*, 1995, **69**, 119-120.
- 32 D. Geethalakshmi, N. Muthukumarasamy and R. Balasundaraprabhu, *J. Mater. Sci.-Mater. Electron.*, 2015, **26**, 7797-7803.
- 33 L. Zhang, C. Zhang and J. Lian, *Biosens. Bioelectron.*, 2008, **24**, 690-695.
- 34 S. Mu and J. Kan, *Synth. Met.*, 2002, **132**, 29-33.
- 35 Y. R. Park, J. H. Doh, K. Shin, Y. S. Seo, Y. S. Kim, S. Y. Kim, W. K. Choi and Y. J. Hong, *Org. Electron.*, 2015, **19**, 131-139.
- 36 H. Tang, Y. Liu, B. Li, B. Shang, J. Yang, C. Zhang, L. Yang, K. Chen, W. Wang and J. Liu, *Bioact. Mater.*, 2021, **6**, 4758-4771.
- 37 M. Sniechowski, D. Djurado, B. Dufour, P. Rannou, A. Pron and W. Luzny, *Synth. Met.*, 2004, **143**, 163-169.
- 38 A. John, S. Palaniappan, D. Djurado and A. Pron, *J Polym. Sci., Polym. Chem.*, 2008, **46**, 1051.
- 39 J. Yue, Z. H. Wang, K. R. Cromack, A. J. Epstein and A. G. MacDiarmid, *J. Am. Chem. Soc.*, 1991, **113**, 2665-2671.
- 40 H. Bai, Y. Xu, L. Zhao, C. Li and G. Shi, *Chem. Commun.*, 2009, **2009**, 1667-1669.
- 41 C. Park, H. Yoon, M. A. Zahed, S. Zhang, S. Yoon, D. Kim, D. Kim and J. Park, *IEEE Sens. J.*, 2022, **22**, 11213-11221.



- 42 Y. Liang, A. Offenhäusser, S. Ingebrandt and D. Mayer, *Adv. Healthc. Mater.*, 2021, **10**, 2100061.
- 43 I. Nasuno, Japanese Patent JP5303107, issued June 28, 2013.



## Data Availability Statement

### Organic electrochemical transistor-based biosensors using doped polyaniline

Ryotaro Kawamura, Waner He\*, Atsushi Isobe, Haoqin Zhang, Nanase Ikeda, Yuhei Hayamizu, and Tsuyoshi Michinobu\*

Data availability:

The data that support the findings of this study are available from the corresponding author upon reasonable request.

